Fully Automatic Method for 3D T1-Weighted Brain Magnetic Resonance Images Segmentation

Bouchaib CHERRADI *cherradi1@hotmail.com*
Ph. D student
UFR: MCM&SCP
F.S.T, BP 146, Mohammedia, Morocco.

Omar BOUATTANE *bouattane@hotmail.com*
Professor
E.N.S.E.T, Informatics Department
Hassan II St, Mohammedia, Morocco.

Mohamed YOUSSFI *med@youssfi.net*
Ph. D student
F.S, Information Processing Department
Mohamed V University, Rabat. Morocco.

Abdelhadi RAIHANI *abraihani@yahoo.fr*
Ph. D student
F.S, Information Processing Department
Hassan II University, Mohammedia. Morocco.

Abstract

Accurate segmentation of brain MR images is of interest for many brain disorders. However, due to several factors such noise, imaging artefacts, intrinsic tissue variation and partial volume effects, brain extraction and tissue segmentation remains a challenging task. So, in this paper, a full automatic method for segmentation of anatomical 3D brain MR images is proposed. The method consists of many steps. First, noise reduction by median filtering is done; second segmentation of brain/non-brain tissue is performed by using a Threshold Morphologic Brain Extraction method (TMBE). Then initial centroids estimation by gray level histogram analysis is executed, this stage yield to a Modified version of Fuzzy C-means Algorithm (MFCM) that is used for MRI tissue segmentation. Finally 3D visualisation of the three clusters (CSF, GM and WM) is performed. The efficiency of the proposed method is demonstrated by extensive segmentation experiments using simulated and real MR images. A confrontation of the method with similar methods of the literature has been undertaken trough different performance measures. The MFCM for tissue segmentation introduce a gain in rapidity of convergence of about 70%.

Keywords: Noise Reduction, Brain Extraction, Clustering, MRI Segmentation, Performance Measures.

1. INTRODUCTION

Magnetic resonance (MR) imaging has been widely applied in biological research and diagnostics, primarily because of its excellent soft tissue contrast, non-invasive character, high spatial resolution and easy slice selection at any orientation. In many applications, its segmentation plays an important role on the following sides: (a) identifying anatomical areas of interest for diagnosis, treatment, or surgery planning paradigms; (b) pre-processing for multimodality image registration; and (c) improved correlation of anatomical areas of interest with localized functional metrics [1].

Intracranial segmentation commonly referred to as brain extraction, aims to segment the brain tissue (cortex and cerebellum) from the skull and non-brain intracranial tissues in magnetic

resonance (MR) images of the brain. Brain extraction is an important pre-processing step in neuroimaging analysis because brain images must typically be skull stripped before other processing algorithms such as registration, tissue classification or bias field correction can be applied [2-6]. In practice, brain extraction is widely used in neuroimaging analyses such as multi-modality image fusion and inter-subject image comparisons [2], [3]; examination of the progression of brain disorders such as Alzheimer's Disease [7, 8], multiple sclerosis [9-12] and schizophrenia [13], [14]; monitoring the development or aging of the brain [15], [16]; and creating probabilistic atlases from large groups of subjects [2]. Numerous automated brain extraction methods have been proposed [17-24]. However, the performance of these methods, which rely on signal intensity and signal contrast, may be influenced by numerous factors including MR signal inhomogeneities, type of MR image set, stability of system electronics, and extent of neurodegeneration in the subjects studied. In [25] we have proposed simple hybrid method, based on optimal thresholding and mathematical morphology operators for extracting brain tissues from 2D T1-weighted cerebral MRI images.

From the pattern recognition point of view, the tissue segmentation stage is to classify a set of elements defined by a set of features among which a set of classes can be previously known. In the MRI segmentation domain, the vector pattern X corresponds to the gray level of the studied point (pixel or voxel). From these approaches, one distinguishes the supervised methods where the class features are known a priori, and the unsupervised ones which use the features auto-learning. From this point of view, several algorithms have been proposed such as: c-means [26], fuzzy c-means (FCM) [27], adaptive fuzzy c-means [28], modified fuzzy c-means [29] using illumination patterns and fuzzy c-means combined with neutrosophic set [30].

Segmentation is a very large problem; it requires several algorithmic techniques and different computational models, which can be sequential or parallel using processor elements (PE), cellular automata or neural networks. In [31], we have presented Parallel implementation of c-means clustering algorithm to demonstrate the effectiveness and how the complexity of the parallel algorithm can be reduced in the reconfigurable mesh computer (RMC) computational model. In [32] the authors present the design, the modelling and the realisation of an emulator for this massively parallel re-configurable mesh computer.

Fully automatic brain tissue segmentation of magnetic resonance images (MRI) is of great importance for research and clinical study of much neurological pathology. The accurate segmentation of MR images into different tissue classes, especially gray matter (GM), white matter (WM) and cerebrospinal fluid (CSF), is an important task. Moreover, regional volume calculations of these tissues may bring even more useful diagnostic information. Among them, the quantization of gray and white matter volumes may be of major interest in neurodegenerative disorders such as Alzheimer disease, in movements disorders such as Parkinson or Parkinson related syndrome, in white matter metabolic or inflammatory disease, in congenital brain malformations or prenatal brain damage, or in post traumatic syndrome. The automatic segmentation of brain MR images, however, remains a persistent problem. Automated and reliable tissue classification is further complicated by the overlap of MR intensities of different tissue classes and by the presence of a spatially smoothly varying intensity inhomogeneity.

In this paper we present fully automatic method for brain MRI volume segmentation. The system combines noise reduction by median filtering, the proposed TMBE method for non brain tissue removal, initial centroids estimation by gray level histogram analysis, and Fuzzy C-means Algorithm for tissue segmentation. Extensive experiments using simulated and real MR image data show that the proposed method can produce good segmentation results. Quantitative evaluation of the efficiency of the proposed method for brain extraction and tissue segmentation is confronted to some well known methods trough standard performance measure in the literature.

The reminder of this paper is organized as follows. Section 2 presents the pre-processing procedure in witch we represent our proposed method for brain extraction (TMBE) and a procedure for noise removing. Tissue classification method and performance measure are presented in section 3. Simulation results for the two main stages in the fully automatic method

for T1-weighted MRI images (Brain Extraction and tissue classification) are introduced in Section 4. Finally, conclusion and perspectives are given in section 5.

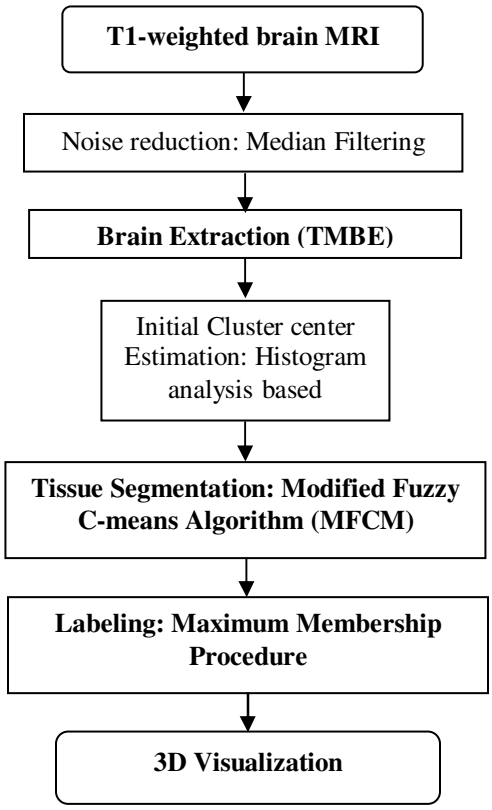

FIGURE 1: Global segmentation scheme.

2. PRE-PROCESSING

2.1. Noise reduction: Filtering

This pre-processing stage performs a non linear mapping of the grey level dynamics for the image. This transform consists in the application of a 3x3 median filter. The use of median filtering derives from the nature of the noise distribution in the MR images. The main source of noise in this kind of images is due to small density variations inside a single tissue which tend to locally modify the RF emission of the atomic nuclei during the imaging process. Such variations derive either from casual tissue motions or by external RF interferences and they assume a salt-and-pepper appearance. The median filter is a non-derivative low-pass one that removes efficiently this kind of disturb, allows homogeneous regions to become denser, thus improving clustering performance. The choice of the neighbourhood size derives from the need to avoid small regions to be confused with noise. Several approaches use complex models of the noise and perform anisotropic filtering because the noise distribution is, to some extent, oriented with the spatial direction of the RF atomic emission across the image. Here, the main concern is to reduce noise and make the single tissues more homogeneous.

2.2 Brain Extraction

The Brain extraction problem is a difficult task, which aims at extracting the brain from the skull, eliminating all non-brain tissue such as bones, eyes, skin, fat… This will allow us to simplify the segmentation of the brain tissues.

2.2.1 Some Previous Brain Extraction Techniques

2.2.1.1 Brain Extraction Tool (BET)

BET [21] is developed by FMRIB (Oxford Centre for Functional Magnetic Resonance Imaging of the Brain) and is available at http://www.fmrib.ox.ac.uk/fsl/ for research purposes. In BET, the intensity histogram is processed to find "robust" lower and upper intensity values for the image, and a rough brain/non-brain threshold is determined. The center-of-gravity of the head image is found, along with the rough size of the head in the image. Next a triangular tessellation of a sphere's surface is initialized inside the brain, and allowed to slowly deform, one vertex at a time, following forces that keep the surface well-spaced and smooth, whilst attempting to move towards the brain's edge. If a suitably clean solution is not arrived at then this process is re-run with a higher smoothness constraint.

2.2.1.2 Brain Surface Extractor (BSE)

BSE [22] is developed by NeuroImaging Research Group, University of Southern California and the executable is available from http://neuroimage.usc.edu/BSE/. BSE is an edge based method that employs anisotropic diffusion filtering. Edge detection is implemented using a 2D Marr-Hildreth operator, employing low-pass filtering with a Gaussian kernel and localization of zero crossings in the Laplacian of the filtered image. The final step is morphological processing of the edge map.

2.2.1.3 McStrip (Minneapolis Consensus Stripping)

McStrip [16], [17] is developed by International Neuroimaging Consortium (INC) and is available for download at http://www.neurovia.umn.edu/incweb/McStrip_download.html. McStrip is initialized with a warp mask using AIR (http://bishopw.loni.ucla.edu/AIR5/), and dilates the AIR mask to form a Coarse Mask. It then estimates a brain/ non-brain threshold based on the intensity histogram, and automatically adjusts this threshold to produce a Threshold Mask. The volume of tissue within the Threshold Mask determines the choice of the BSE Mask from among a suite of 15 masks computed using parameter combinations spanning both smoothing and edge parameters. The final, McStrip Mask is a union of the Threshold and BSE masks after void filling and smoothing.

2.2.2 Threshold Morphologic Brain Extraction (TMBE)

Our simple and effective method is divided in five steps [25]

2.2.2.1 Binarisation by Thresholding

This step is based on global binary image thresholding using Otsu's method [33]. Figure 2-b shows a result of this operation.

2.2.2.2 Greatest Connected Component Extraction

A survey based on a statistical analysis of the existing connected components on the binary image, permits to extract the region whose area is the biggest. Figure 2-c shows a result of this operation.

2.2.2.3 Filling the Holes

The remaining holes in the binary image obtained in step 2, containing the greatest connected component, are filled using morphologic operation consisting of filling holes in the binary image. A hole is a set of background voxels within connected component. The result of this operation is shown in figure 2-d.

2.2.2.4 Dilatation

This morphologic operation consists of eliminating all remaining black spots on the white surface of the image. These spots are covered by the dilatation of the white parts. This carried out by moving a square structuring element of size (S*S) on binary image and applying logical OR operator on each of the (S^2-1) neighbouring pixels (figure 2-e). Here we choose S=3.

2.2.2.5 Brain Extracting

The region of interest is the brain. To extract this region we use the AND operator between the original filtered image (figure 2-a) and the binary mask obtained in last step as is shown in figure 2-f. The non-brain tissues are obtained by applying AND operator between the image in figure 2a and the logical complement of the mask in figure 2e, the result is in figure 2-g.

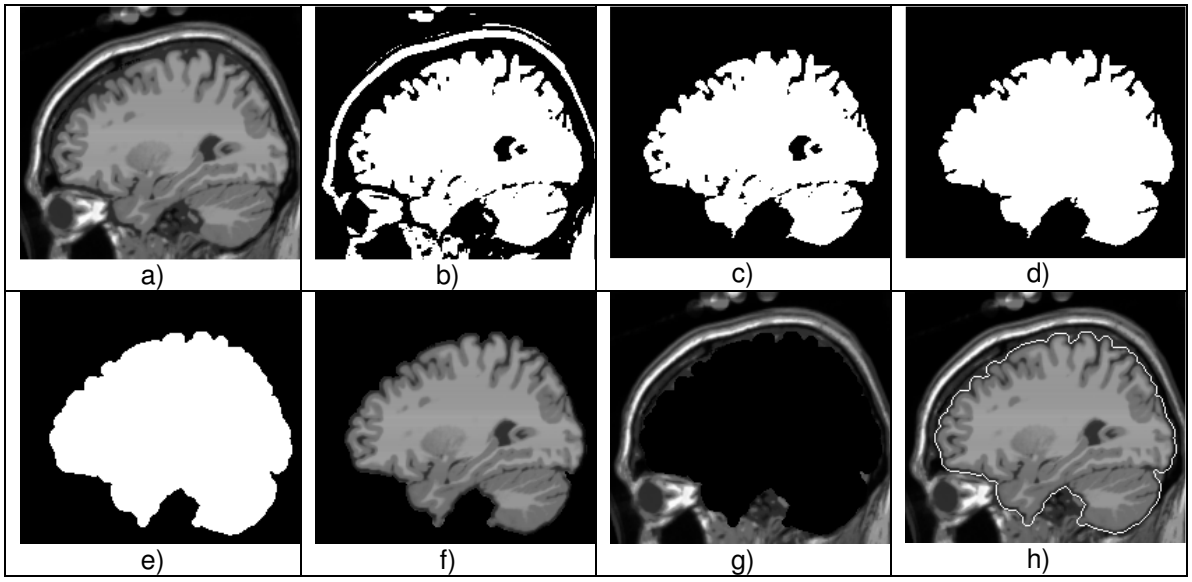

FIGURE 2: TMBE steps on sagitale slice number 120/181 from normal brain simulated phantom [40].

The figure 2-h shows the region of interest corresponding to the effective brain tissues in original MRI delimited by contour.

2.3. Histogram Based Centroids Initialization

Clustering algorithms requires an initialisation of the centroids values. Usually, this is randomly made. However, an adequate selection permits generally to improve the accuracy and reduces considerably the number of required iterations to the convergence of these algorithms.
Among the methods used to estimate initial cluster values in the image, we used the histogram information analysis [25], [34].

The choice of the class number is done according to the quantity of information that we want to extract from the image. In our case this number is known in advance since we have extract three clusters from normal images (CSF, GM and WM).

2. TISSUE CLASSIFICATION

3.1. Image Segmentation

The objective of image segmentation is to divide an image into meaningful regions. Errors made at this stage would affect all higher level activities. In an ideally segmented image, each region should be homogeneous with respect to some criteria such as gray level, color or texture, and adjacent regions should have significantly different characteristics or features. More formally, segmentation is the process of partitioning the entire image into C regions $\{R_i\}$ such that each R_i is homogeneous with respect to some criteria. In many situations, it is not easy to determine if a voxel should belong to a region or not. This is because the features used to determine homogeneity may not have sharp transitions at region boundaries. To alleviate this situation, we inset fuzzy set concepts into the segmentation process. In fuzzy segmentation, each voxel is assigned a membership value in each of the C regions. If the memberships are taken into

account while computing properties of regions, we obtain more accurate estimates of region properties. One of the known techniques to obtain such a classification is the FCM algorithm.

3.2. Clustering: Modified FCM Algorithm

The fuzzy c-means (FCM) clustering algorithm was first introduced by DUNN [35] and later was extended by BEZDEK [36]. Fuzzy C-means (FCM) is a clustering technique that employs fuzzy partitioning such that a data point can belong to all classes with different membership grades between 0 and 1.

The aim of FCM is to find C cluster centers (centroids) in the data set $X = \{x_1, x_2, ...x_N\} \subseteq R_p$ that minimize the following dissimilarity function:

$$J_{FCM} = \sum_{i=1}^{C} J_i = \sum_{i=1}^{C} \sum_{j=1}^{n} u_{ij}^{\ m} d^2_{(V_i, x_j)} \qquad (1)$$

u_{ij}: Membership of data x_j in the cluster V_i;
V_i : Centroid of cluster i;
$d_{(Vi,xj)}$: Euclidian distance between i^{th} centroid (V_i) and j^{th} data point x_j;
$m \in [1,\infty[$: Fuzzy weighting exponent (generally equals 2).
N: Number of data.
C: Number of clusters, $2 \le C \le N$.
p: Number of features in each data x_j.

With the constraints:

$$u_{ij} \in [0,1], \forall i, j \qquad (2a)$$

$$\sum_{i=1}^{C} u_{ij} = 1, \forall j = 1,..., N \qquad (2b)$$

$$0 < \sum_{j=1}^{N} u_{ij} < N, \forall i = 1,..., C \qquad (2c)$$

To reach a minimum of dissimilarity function there are two conditions.

$$V_i = \frac{\sum_{j=1}^{N} u_{ij}^{\ m} x_j}{\sum_{j=1}^{N} u_{ij}^{\ m}} \qquad (3)$$

$$u_{ij} = \frac{1}{\sum_{k=1}^{C} \left(\frac{d_{ij}}{d_{kj}} \right)^{2/(m-1)}} \qquad (4)$$

We have modified this iterative algorithm to include the proposed procedure for estimating initial centroids with histogram analysis; this algorithm is in the following steps.

Step 0. *Estimate the number of clusters C according to the procedure in section 2-3, choose the correspondent's gray level values as initial values of cluster centres $V^{(0)}$, Choose fuzzification parameter m ($1 < m < \infty$) m=2, and choose threshold ε>0. Initialize the membership matrix (U) according to the constraints of equations 2a, 2b and 2c.*

At iteration Ni

{ **Step 1.** *Calculate centroids $V^{(Ni)}$ using Equation (3).*

Step 2. *Compute dissimilarity function J_{Ni} using equation (1). If its improvement over previous iteration ($J_{Ni} - J_{Ni-1}$) is below a threshold ε>0, Go to Step 4.*

Step 3. *Compute a new membership matrix (U_{Ni}) using Equation (4). Go to Step 1.*

Step 4. *Stop. }*

3.3. Performance Measures

To compare the performance of various segmentation techniques, we compute different coefficients reflecting how well two segmented regions match. The manually segmented regions are used as a gold standard (Truth Verity), and the automatically segmented ones are compared to them. To provide comparison between methods, we use a different performance measure:

3.3.1. Jaccard Similarity Coefficient

According to [37] the Jaccard similarity coefficient JSC is formulated as:

$$JSC = Card(R_1 \cap R_2) / Card(R_1 \cup R_2) \qquad (5)$$

Where R_1 is the automatically segmented region, R_2 is the correspondent region of the manually segmented image, and *Card(X)* denotes the number of voxels in the region X. A JSC of 1.0 represents perfect overlap, whereas an index of 0.0 represents no overlap. JSC values of 1.0 are desired.

3.3.2. Dice Similarity Coefficient [38]

Dice Similarity Coefficient is used to show the similarity level of automatically segmented region to manual segmented one. The Dice coefficient is defined as:

$$DSC = 2 * Card(R_1 \cap R_2) / Card(R_1 + R_2) \qquad (6)$$

Where R_1 is the automatically segmented region, R_2 is the region of the manually segmented image, and Card(X) denotes the number of voxels in the region X. A DSC of 1.0 represents perfect overlap, whereas an index of 0.0 represents no overlap. DSC values of 1.0 are desired.

3.3.3. Sensitivity and Specificity [39]

We also compute the sensitivity and specificity coefficient of the automated segmentation result using the manually segmented mask. The Sensitivity is the percentage of voxels recognized by the algorithm (Equation 7). The Specificity is the percentage of non recognized voxels by the algorithm (Equation 8).

$$Sensitivity = \frac{TP}{TP + FN} \qquad (7)$$

$$Specificity = \frac{TN}{TN + FP} \qquad (8)$$

Where TP and FP stand for true positive and false positive, which were defined as the number of voxels in R_1 correctly and incorrectly classified as R_2 by the automated algorithm. TN and FN stand for true negative and false negative, which were defined as the number of voxels in R_1 correctly and incorrectly classified as non R_2 by the automated algorithm.

4. RESULTS AND DISCUSSION

4.1. Brain Extraction

To prove the effectiveness of the proposed method for the skull stripping problem we have massively experiment TMBE using simulated and real MR image data in different modalities of acquisition. The figure 3 shows some samples of pre-processed images.

To evaluate the TMBE method we used a set of simulated and real volumes given from reference sites, they are presented as follows:

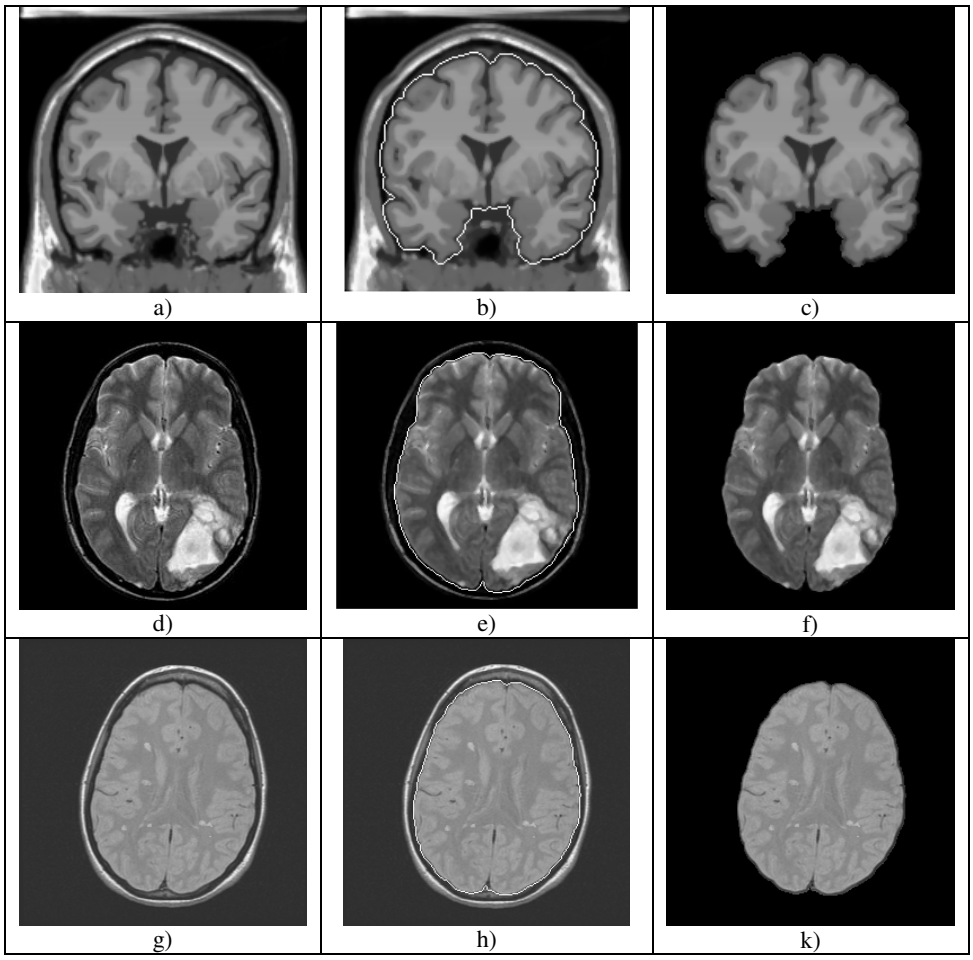

FIGURE 3: Some examples of pre-processed images by the proposed TMBE method (for Qualitative evaluation). a)-c) Simulated T1-weighted image number 127/217 in coronal direction, d)-f) T2-weighted image with tumor, g)-k) PD-weighted image with Multiple Sclerosis (MS) lesion.

- 20 simulated volumes of size 181x217x181 voxels given from the Brainweb simulated brain database [40] and their given manual segmentation (determined by union of the three tissues to form the correspondent region of interest (Brain) for each volume). This T1-weighted data are provided with *1mm×1mm×1mm* in spacing.

- 18 real T1-weighted volumes which were acquired coronally with size 256×256×128 voxels and *0.94mm×0.94mm×1.5mm* as spatial resolution from the International Brain Segmentation Repository IBSR V2.0 [41]. The MR brain data sets and their manual segmentations in three tissues by expert radiologists were provided by the Center for Morphometric Analysis at Massachusetts General Hospital (The image data sets used were named IBSR_01 through IBSR_18).

T1-weighted modality, that belong to the fastest MRI modalities available, are often preferred, since they offer a good contrast between gray (GM) and white cerebral matter (WM) as well as between GM and cerebrospinal fluid (CSF).

To compare the performance of TMBE with three well known brain extraction techniques BET [21], BSE [22] and McStrip [23, 24] we compute the different coefficients described in section 3.3. The manually segmented brains are used as a Truth Verity (TV), and the automatically extracted brains by the proposed method TBME are compared to them.

Quantitative comparison of the proposed Brain Extraction method TMBE to these brain extraction methods for two real datasets (IBSR_07 and IBSR_12) is summarised in Table.1 and Table.2. The values indicated in tables are average values for multiple essays.

Notice that, we have implemented the method in MATLAB 7.8 and have been used on a Pentium IV personal computer (Intel) with 2.6 GHz, 1024 MB of main memory, and an NVIDIA Geforce 7900 graphics card with 256 MB of graphics memory.

	JSC	DSC	Sensitivity	Specificity	time
BET [21]	0.81	0.76	0.603	0.912	3 min
BSE [22]	0.82	0.88	0.607	0.973	2 min
McStrip [23,24]	0.80	0.84	0.600	0.903	6 min
TMBE	0.80	0.87	0.599	0.901	4 min

TABLE 1: Different similarity index calculated for brain extraction of ISBR_7.

	JSC	DSC	Sensitivity	Specificity	time
BET [21]	0.85	0.78	0.600	0.902	3 min
BSE [22]	0.86	0.89	0.622	0.923	2 min
McStrip [23,24]	0.82	0.82	0.610	0.913	6 min
TMBE	0.84	0.86	0.591	0.923	4 min

TABLE 2: Different similarity index calculated for brain extraction of ISBR_12.

The comparison of TMBE with the three brain extraction techniques against expertly hand stripped T1-weighted MRI volumes revealed that TMBE method gives comparable results to BSE and BET in term of accuracy but with lowest time processing (creating mask in about 4 min). But when compared with McStrip technique it is faster.

4.2 Tissues Classification

The tissues classification aims to divide the extracted volume by TMBE in three clusters: Cerebrospinal fluid (CSF), gray matter (GM), and white matter (WM). The background voxels are removed by simple thresholding before the clustering starts.

4.2.1 Classification Results

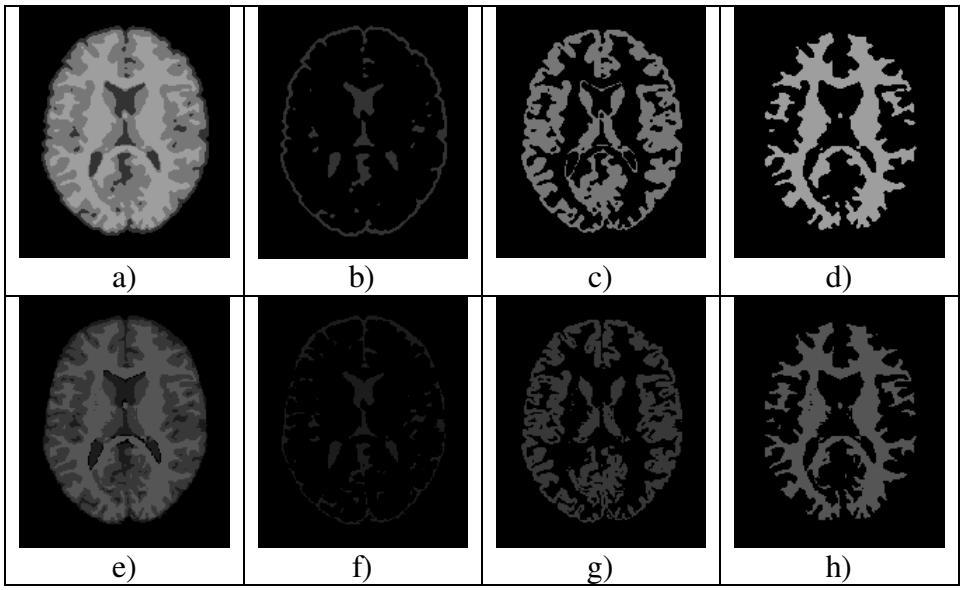

FIGURE 4: Example of segmentation results comparison. a) Segmented image by the proposed method, b) Cerebrospinal fluid (CSF) cluster, c) Gray matter (GM) cluster and d) The white matter (WM) cluster. e) Truth Verity image. f), g) and h) Manual segmentation of the same brain tissues (Brainweb).

For qualitative evaluation, Figure.4 shows segmentation results of axial T1-weighted slice of number 84 in axial direction obtained from the web site Brainweb [40] its about t1_icbm_normal_1mm_pn0_rf0 volume file which we call **Dataset1**, the image was segmented in three clusters (Truth Verity). It is very clear from this figure that the separation of the three clusters is very effective in comparison with the correspondent's results (TV).

4.2.2 Parameters Dynamic of the MFCM.

Table.3 shows the Different parameters states of the Modified FCM clustering by starting from centroids: (C1: CSF, C2: GM and C3: WM) = (53.50, 115.01 and 150.50), corresponding to the results in figure 4 and figure 5.

	Value of each Cluster			Number of voxels in each Cluster			ObjFcn value
Ni	CSF	GM	WM	Card(CSF)	Card(GM)	Card(WM)	J(Ni)
1	53.50	115.01	150.50	2364	7270	7617	1299906.70
2	52.93	113.42	151.71	2322	7312	7617	1293634.77
3	52.51	113.05	151.78	2288	7346	7617	1293020.71
4	52.31	112.92	151.76	2288	7346	7617	1292923.43
5	52.23	112.87	151.74	2288	7346	7617	1292907.25
6	52.20	112.86	151.74	2288	7346	7617	1292904.56

TABLE 3: Different parameters states of the clustering method starting from centroids: (C1: CSF, C2: GM and C3: WM) = (53.50, 115.01and 150.50).

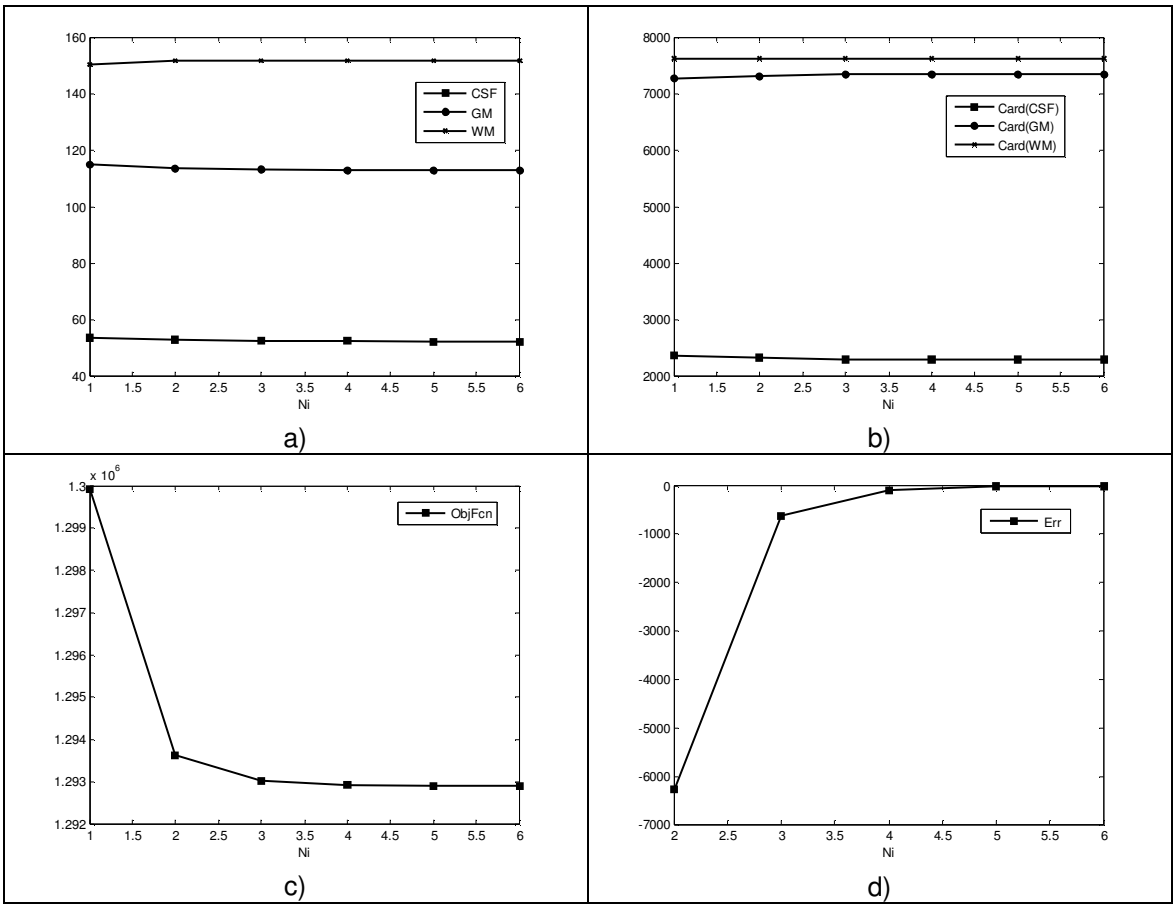

FIGURE 5: Dynamic of different clustering parameters:
a) Centroids starting from (C1, C2, C3) = (35.50, 115.01, 150.50) as results of histogram analysis,
b) Cardinality of each tissue, c) Value of objective function J(Ni), d) Value of Err=(J(Ni)-J(Ni-1)).

In figure.5 we present the dynamic of different clustering parameters using the results of histogram analysis leading to a centroids initialization of the extracted region of interest consisting of brain tissues that we want segment. These results correspond to variation trough the iterations of the clusters centroids values, the cardinality of each cluster, the FCM objective function J(Ni) and the difference between two successive objective function values (J(Ni)-J(Ni-1)) used as criteria for convergence.

As shown in figure. 5 and trough many experiment done on different images, the rapidity of the method is much enhanced (6 iterations) in comparison with the case of random initialisation of the cluster centroids that is practiced in standard FCM clustering (about 20 iterations).

Table.3 shows the dynamic of different parameters states of the modified FCM clustering starting from centroids: (C1: CSF, C2: GM and C3: WM) = (53.50, 115.01 and 150.50), corresponding to the results presented in figures 4 and 5, this values of initial centroids are obtained by histogram analysis described in section 2-3.

In this table we show that we can stop iterative procedure more early, since the clusters cardinalities don't change anymore from the iteration number 3. The clusters centres have their tower change with very small amounts.

4.2.3 Noise Robustness of the Proposed Method

To evaluate the robustness of the proposed method for tissue classification to the presence of noise, we used **Dataset1** with additional noise levels: 0%, 1%, 3%, 5%, 7% and 9%.

Dataset1: t1_icbm_normal_1mm_pn0_rf0 [40], is simulated normal brain phantom of 181x217x181 voxels with $1mm^3$ for each voxel without any noise or intensities inhomogeneity.

Noise	JSC	DSC	Sensitivity	Specificity
0%	0.942	0.955	0.757	0.895
1%	0.948	0.953	0.743	0.895
3%	0.919	0.943	0.732	0.899
5%	0.893	0.929	0.715	0.899
7%	0.854	0.922	0.704	0.897
9%	0.849	0.908	0.688	0.897

TABLE 4: Performance measures for Modified FCM Clustering results of WM tissue (Dataset1).

In table.4 and table.5 we summarise the performance measure results calculated for segmented GM and WM of different variants of **Dataset1** obtained with additional noise of different amounts.

Noise	JSC	DSC	Sensitivity	Specificity
0%	0.952	0.975	0.657	0.897
1%	0.948	0.973	0.653	0.887
3%	0.929	0.963	0.642	0.880
5%	0.903	0.949	0.625	0.870
7%	0.874	0.932	0.614	0.850
9%	0.849	0.918	0.598	0.840

TABLE 5: Performance measures for Modified FCM Clustering results of GM tissue (Dataset1).

4.2.4 Visualisation of 3D Rendered Surface.

To appreciate the segmentation results obtained slice by slice, in 3D space, we export our segmentation results to ANALYZE 10.0 that is a comprehensive and interactive package for multidimensional image visualization, processing and analysis developed by The Biomedical Imaging Resource at Mayo Clinic, Rochester, MN [42].

The figure.6 shows 3D rendered surface of the segmentation results for the three tissues extracted from Dataset1. For the CSF we have limited the visualisation to the lateral ventricles.

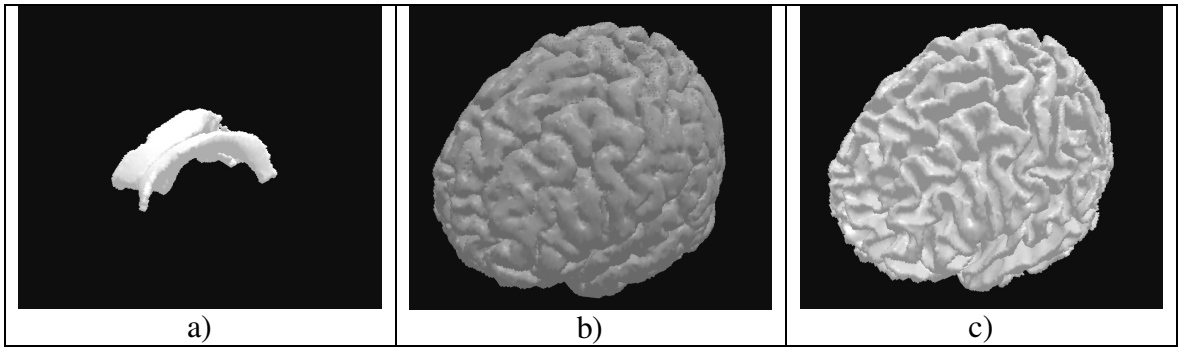

FIGURE 6: 3D visualization of rendered surface for segmented volume (Dataset1). a) Lateral Ventricular CSF, b) GM, c) WM.

5. CONCLUSION AND PERSPECTIVES

In this paper, we have presented a complete MRI images segmentation method. Unlike other brain segmentation methods described in the literature, the one described in this paper is truly automatic because it does not require a user to determine image-specific parameters, thresholds, or regions of interest.

The automatic proposed method for extracting the brain from the T1-weighted MRI head scans is based on a hybrid processing techniques including global optimal thresholding and mathematical morphology operators. Our quantitative results show that the proposed method achieves comparable performance with synthetic BrainWeb data, and real IBSR V2.0 data against standard techniques such as BSE and BET, and **McStrip.** Our results are also more consistent across the datasets, making the proposed method suited for measuring brain volumes in a clinical setting.

Concerning the tissues classification we used modified FCM that is a clustering technique that utilizes the distance between voxels and cluster centres in the spatial domain to compute the membership function. The modification consists of using the histogram analysis for the determination of initial cluster centroids instead of a random initialization. The segmentation process is achieved in 6 iterations instead of about 20 iterations when we used standard FCM with random initial centroids. This is important improvement (about 70%) especially in our case where we manipulate big quantity of data.

The accuracy and the effectiveness of the fully automatic proposed method for 3D brain MR images segmentation has been evaluated qualitatively and quantitatively, but more work can be done to improve the method that need to be tested on many more data sets to expose unexpected segmentation errors that might occur infrequently. The method should also be tested with more recent images database.

More comprehensive comparison of MFCM with other clustering models will be addressed.
Future work will focus on developing an automatic image based classification system for brain tumor using MRI data of different modalities and taking into account the intensity nonuniformity artefact.

Another improvement in time processing can be gained while modifying the convergence criteria for FCM clustering by considering a threshold on the change of clusters centres instead of calculating the objective function.

An implementation of the proposed method as well as other algorithms for MRI segmentation on massively parallel reconfigurable mesh computer emulator [32] is being finalised.

REFERENCES.

[1] L.P Clarke, R.P Velthijizen, M.A Camacho, J. J Heine, “MRI segmentation methods and applications”, Magnetic Resonance Imaging, Vol. 13, No. 3, pp. 343-368, 1995.

[2] R. P. Woods, S. T. Grafton, J. D. G. Watson, N. L.Sicotte, and J. C. Mazziotta, “Automated image registration: II. Intersubject validation of linear and nonlinear models”, J. of Computer Assisted Tomography, vol. 22, pp: 139-152, 1998.

[3] R. P. Woods, M. Dapretto, N. L. Sicotte, A. W. Toga, and J. C. Mazziotta, “Creation and use of a Talairach-Compatible atlas for accurate, automated, nonlinear intersubject registration, and analysis of functional imaging data”, Human Brain Mapping, vol. 8, pp: 73-79, 1999.

[4] J. Van Horn, T. M. Ellmore, G. Esposito, K. F. and Berman, “Mapping Voxel-based Statistical Power on Parametric Imaging”, NeuroImage, vol. 7, pp: 97-107, 1998.

[5] D. W. Shattuck, S.R. Sandor-Leahy, K. A. Schaper, D. A. Rottenberg, and R. M. Leahy, "Magnetic Resonance Image Tissue Classification Using a Partial Volume Model", NeuroImage, vol. 13, pp: 856-876, 2001.

[6] S. Strother, S. La Conte, L. Kai Hansen, J. Anderson, J. Zhang, S. Pulapura, and D. Rottenberg, "Optimizing the fMRI data-processing pipeline using prediction and reproducibility performance metrics: I. A preliminary group analysis", NeuroImage, vol. 23, pp:196-207, 2004.

[7] H. Rusinek, M. J. de Leon, A. E. George, L. A. Stylopoulos, R. Chandra, G. Smith, T. Rand, M. Mourino, and H. Kowalski, "Alzheimer disease: measuring loss of cerebral gray matter with MR imaging", Radiology, vol. 178, pp: 109-114, 1991.

[8] P. M Thompson, M. S. Mega, R. P. Woods, C. I. Zoumalan, C. J. Lindshield, R. E. Blanton, J. Moussai, C. J. Holmes, J. L. Cummings, and A. W. Toga, "Cortical change in Alzheimer's disease in detected with a disease specific population-based brain atlas", Cerebral Cortex vol. 11, pp: 1-16, 2001.

[9] R. A. Bermel, J. Sharma, C. W. Tjoa, S. R. Puli, and R. Bakshi, "A semiautomated measure of whole- brain atrophy in multiple sclerosis", Neurological Sciences, vol. 208, pp: 57-65, 2003.

[10] M. A. Horsfield, M. Rovaris, M. A. Rocca, P. Rossi, R. H. B. Benedict, M. Filippi, and R. Bakshi, "Whole-brain atrophy in multiple sclerosis measured by two segmentation processes from various MRI sequences", Neurological Sciences, vol. 216, pp: 169-177, 2003.

[11] R. Zivadinov, F. Bagnato, D. Nasuelli, S. Bastianello, A. Bratina, L. Locatelli, K. Watts, L. Finamore, A. Grop, M. Dwyer, M. Catalan, A. Clemenzi, E. Millefiorini, R. Bakshi, and M. Zorzon, M., " Short-term brain atrophy changes in relapsing-remitting multiple sclerosis", Neurological Sciences, vol. 223, pp: 185-193, 2004.

[12] J. Sharma, M. P. Sanfilipo, R. H. B. Benedict, B. Weinstock-Guttman, F. E. Munschauer, and R. Bakshi, "Whole-brain atrophy in multiple sclerosis measured by automated versus semi-automated MR imaging segmentation", Neuroradiology, vol. 25, pp: 985-996, 2004.

[13] K. L. Narr, P. M. Thompson, P. Szeszko, D. Robinson, S. Jang, R. P. Woods, S. Kim, K. M. Hayashi, D. Asunction, A. W. Toga, and R. M. Bilder, "Regional specificity of hippocampal volume reductions in first episode schizophrenia", NeuroImage, vol. 21, pp: 1563- 1575, 2004.

[14] P. Tanskanen, J. M. Veijola, U. K. Piippo, M. Haapea, J. A. Miettunen, J. Pyhtinen, E. T. Bullmore, P. B. Jones, and M. K. Isohanni, "Hippocampus and amygdale volumes in schizophrenia and other psychoses in the Northern Finland 1966 birth cohort". Schizophrenia Research, vol. 75, pp: 283-294, 2005.

[15] T. L. Jernigan, S. L. Archibald, C. Fennema-Notestine, A. C. Gamst, J. C. Stout, J. Bonner, and J. R. Hesselink, "Effects of age on tissues and regions of the cerebrum and cerebellum", Neurobiology of Aging, vol. 22, pp: 581-594, 2001.

[16] R. E. Blanton, J. G. Levitt, J. R. Peterson, D. Fadale, M.L. Sporty, M. Lee, D. To, E. C. Mormino, P. M.Thompson, J. T. McCracken, and A. W. Toga, "Gender differences in the left inferior frontal gyrus in normal children", NeuroImage, vol. 22, pp: 626-636, 2004.

[17] A.M. Dale AM, B. Fischl , and M. Sereno, "Cortical surface-based analysis. Segmentation and surface reconstruction", Neuroimage, vol. 9, pp: 179-94, 1999.

[18] H. Hahn, and H-O. Peitgen, "The skull stripping problem in MRI solved by a single 3D watershed transform", MICCAI, LNCS 1935, pp: 134-143, 2000.

[19] S. Sandor, and R. Leahy, "Surface-based labeling of cortical anatomy using a deformable database", IEEE Transactions on Medical Imaging, vol. 16, pp: 41-54, 1997.

[20] F. Segonne, A. M. Dale, E. Busa, M. Glessner, D. Salat, H. K. Hahn, and B. Fischl, "A hybrid approach to the skull stripping problem in MRI", Neuroimage, vol. 22, pp :1060-75, 2004.

[21] S. M. Smith, "Fast robust automated brain extraction", Human Brain Mapping, vol. 17, pp: 143-55, 2002.

[22] Shattuck, D.W., Sandor-Leahy, S.R., Shaper, K.A., Rottenberg, D.A., Leahy, R.M., Magnetic resonance image tissue classification using a partial volume model. NeuroImage. 13 (5), 856–876. 2001.

[23] Rehm K, Shattuck D, Leahy R, Schaper K, Rottenberg DA. "Semi-automated stripping of T1 MRI volumes: I. Consensus of intensity- and edge-based methods". NeuroImage. 9(6) S86, 1999.

[24] Rehm K, Schaper K, Anderson J, Woods R, Stoltzner S, Rottenberg D. "Putting our heads together: a consensus approach to brain/non-brain segmentation in T1-weighted MR volumes". NeuroImage, November, 2003.

[25] B. Cherradi O. Bouattane, M. Youssfi and A. Raihani," Brain Extraction and Fuzzy Tissue Segmentation in Cerebral 2D T1-Weigthed Magnetic Resonance Images". International Journal of Computer Science Issues, Vol. 8, Issue 3, May 2011, In Press

[26] J. B. MacQueen, "Some Methods for classification and Analysis of Multivariate Observations", Proceedings of 5th Berkeley Symposium on Mathematical Statistics and Probability, Berkeley, University of California Press, 1:281-297,1967.

[27] J.S.R. Jang, C. Sun, T.E. Mizutani, Neuro-Fuzzy and Soft Computing, Prentice Hall, pp. 426–427. 1997.

[28] L. Dzung Pham, L.P. Jerry, "An adaptative fuzzy c-means algorithm for image segmentation in the presence of intensity inhomogeneities", Pattern Recognition Letters 20 57–68,1999.

[29] L. Ma, R.C. Staunton, "A modified fuzzy c-means image segmentation algorithm for use with uneven illumination patterns", Pattern Recognition 40 3005–3011, 2007.

[30] Y. Guo, H.D. Cheng, W. Zaho, Y. Zhang, "A novel image segmentation algorithm based on fuzzy c-means algorithm and neutrosophic set", in: Proceeding of the 11th Joint Conference on Information Sciences, Atlantis Press, 2008.

[31] O. Bouattane, B. Cherradi, M. Youssfi and M.O. Bensalah. "Parallel c-means algorithm for image segmentation on a reconfigurable mesh computer". Parallel Computing, Volume 37, Issues 4-5, Pages 230-243, April-May 2011.

[32] M. Youssfi, O. Bouattane, M.O. Bensalah, "A massively parallel re-configurable mesh computer emulator: design, modeling and realization", Journal of Software Engineering and Applications vol 3, pp 11–26, 2010.

[33] N. Otsu, "A Threshold Selection Method from Gray-Level Histograms". IEEE Transactions on Systems, Man and Cybernetics, Vol. 9, No. 1, pp. 62-661979.

[34] B. Cherradi, O.Bouattane, M. Youssfi and A. Raihani, "Fuzzy segmentation method for MRI images with spatial information", in the proceeding of Mediterranien Congres of Telecommunications (CMT2010). Casablanca, Morocco. pp 296-299, 2010.

[35] J.C. Dunn, “A fuzzy relative of the ISODATA process and its use in detecting compact well-separated clusters”, Journal of Cybernetics 3(3), pp. 32–57, 1973.

[36] J.C. Bezdek, “Pattern Recognition with Fuzzy Objective Function Algorithms”, Plenum Press, New York 1981.

[37] P. Jaccard, “The distribution of the flora in the alpine zone”. New Phytol. 11 (2), 37–50, 1912.

[38] L. Dice, “Measures of the amount of ecologic association between species”, Ecology, vol. 26, pp: 297- 302, 1945.

[39] MJ. Gardner and DG. Altman, “Calculating confidence intervals for proportions and their differences”. BMJ Publishing Group, pp 28-33, 1989.

[40] http://www.bic.mni.mcgill.ca/brainweb/.

[41] http://www.cma.mgh.harvard.edu/ibsr/.

[42] http://www.mayo.edu/bir/Software/Analyze/Analyze.html.